International Journal of Fluid Machinery and Systems
Vol. 3, No. 1, January-March 2010

Original Paper

Experimental Study and Numerical Simulation of Cavity Oscillation in a Diffuser with Swirling Flow

Changkun Chen[1], Christophe Nicolet[2], Koichi Yonezawa[1], Mohamed Farhat[2], Francois Avellan[2], Kazuyoshi Miyazawa[3], Yoshinobu Tsujimoto[2]

[1]Graduate School of Engineering Science, Osaka University
Machikaneyama 1-3, Toyonaka, 560-8531, Japan
[2]Laboratory for Hydraulic Machines, EPFL - Swiss Federal Institute of Technology
33 bis av. de Cour, Lausanne, CH-1007, Switerland
[3]Nagasaki R&D Center, Mitsubishi Heavy Industries, LTD
Fukahori-machi 5-717-1, Nagasaki, 851-0392, Japan

Abstract

The cavity oscillation with swirling flow in hydraulic power generating systems was studied by a simple experiment and numerical simulation. Several types of fluctuation were observed in the experiment, including the cavitation surge caused by the diffuser effect and the vortex precession by the swirling flow. Both cavitation surge and vortex precession were simulated by CFD. Detailed flow structure was examined through flow visualization and CFD.

Keywords: Draft tube surge, diffuser effect, swirl effect, cavitation.

1. Introduction

Securing stable operation is one of the most important issues in hydraulic power generating systems. In Francis turbines, draft tube surge is the most commonly identified phenomenon. At low flow rate, the precessing motion of the vortex rope in the draft tube is the main cause of draft tube surge [1]-[3]. It has been found that a surge can occur even at full load. The behavior of full load surge in model test is reported by Prenat and Jacob [4] in 1986. Arzola et al. [5] found that in a real plant, modifying the shape of the runner cone can change the frequency of full load surge and the surge can be eliminated by air injection from the runner cone. Koutnik et al. [6] simulated the full load surge by representing the effect of the cavitation in the draft tube by cavitation compliance $C = -\partial V_C / \partial p_D$ and mass flow gain factor $\chi = -\partial V_C / \partial Q_D$, where V_C is the volume of the cavity, p_D and Q_D are pressure and flow rate downstream of the cavity. It was shown that the instability occurs when the absolute value of negative mass flow gain factor is larger than a certain value which depends on the value of cavitation compliance. This model was combined with the numerical analysis software SIMSEN to analyze the full load surge observed in a real plant [7]. Although Ref.[6] and [7] show that full load surge can be successfully simulated by using an appropriate value of mass flow gain factor, the flow mechanism determining the mass flow gain factor was not clarified.

Ref.[8] established a one-dimensional analytical model to clarify the possibility of self-excited oscillation mechanism of the full load draft tube surge. Two sources of draft tube instability have been found. The first is the instability caused by the diffuser effect of draft tube. This destabilizing effect appears for all flow rate and the destabilizing effect increases as the increase of the flow rate. The second source of instability is caused by the swirl downstream of the runner, which destabilizes the system in part load operation and stabilizes in over load operation.

In the previous study [9], the model experimental result with axial inflow was discussed. The pressure fluctuation caused by the cavitation surge occurs with a diffuser and does not occur with a straight pipe. The result validates the diffuser effect on the system instability, which has been predicted by the one-dimensional analysis [8]. In the general case of hydraulic power generating system, swirling flow occurs in the draft tube under off-design operating conditions. In the present study, the effect of swirl was examined by model tests. Numerical computation also simulates the fluctuations and the results are analyzed to explain the experimental observation. However, the destabilizing effect of swirling flow from the runner found in the stability analysis in Ref.[8] occurs only with a rotating runner and cannot be simulated in the present model test with a stationary swirler. It can be shown that the swirl itself has a stabilizing effect on the system instabilities. So, only the local effects of swirl on the flows in a

Received March 19 2010; accepted for publication March 24 2010: Review conducted by Prof. Hyung-Hee Cho. (Paper number O10006K)
Corresponding author: Changkun Chen, chenchangkun@gmail.com

diffuser or a straight pipe are included in the present study.

2. Experimental Facility

Figure 1 shows the framework of experimental facility. The working fluid is fully degassed tap water. The water from the pump is separated to two parts: one part enters the vortex chamber in tangential direction to provide the angular momentum of the swirling flow; the other part enters the vortex chamber in radial direction and offers no angular momentum. The swirl number defined as the ratio of angular momentum flux to linear momentum flux was adjusted by the flow rate ratio. The swirling flow generated in the vortex chamber was supplied into a diffuser or a straight pipe. The pressure in the downstream tank was adjusted to set the cavitation number.

Figure 2 shows the test section and the geometry of the vortex chamber. Four inflows from tangential and axial directions form a swirling flow in the vortex chamber. Then the swirling flow exits the vortex chamber and enters the test section. The total flow rate was kept constant at 150L/min. This results in the Reynolds number $Re = u_i d_i / \nu = 9.8 \times 10^4$ at the inlet of the test section. A conical diffuser and a straight pipe as shown in Fig.3 are tested. At low pressure level, cavity occurs at the center of the swirling flow.

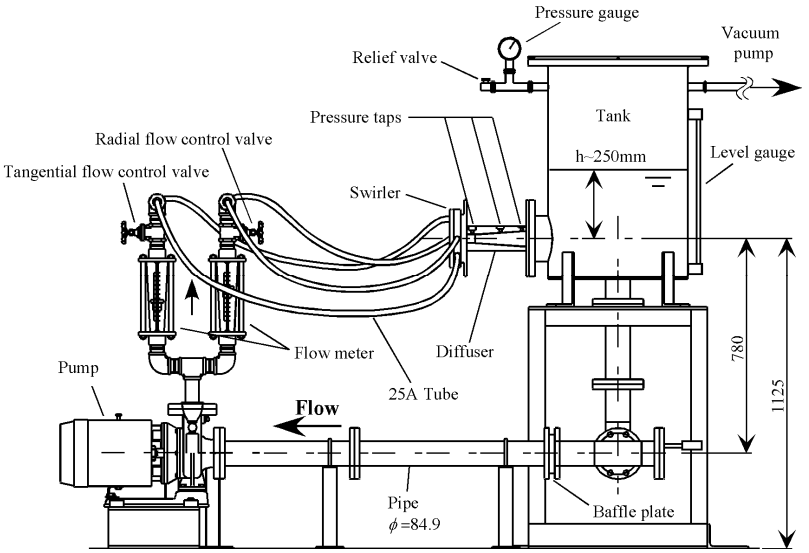

Fig. 1 Schematic of experimental facility with swirling flow

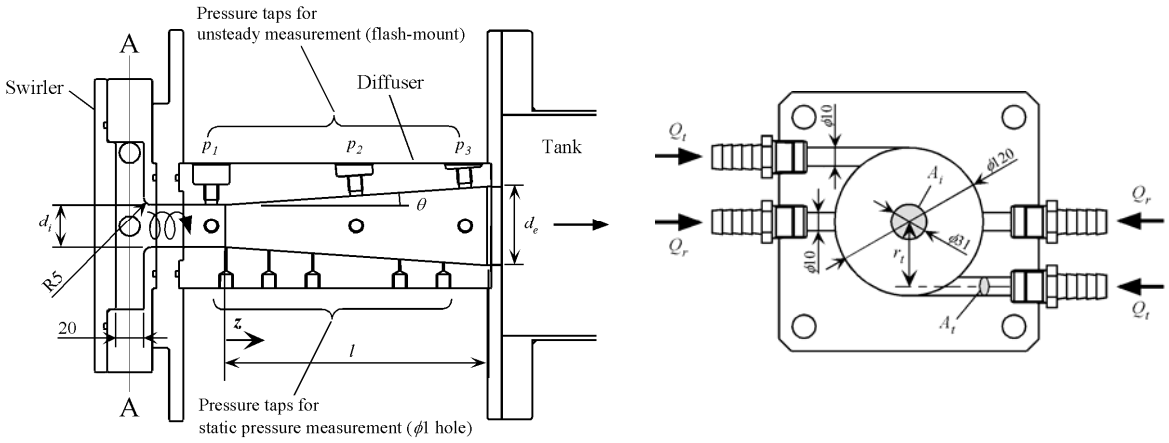

(a) test section (b) A-A section

Fig. 2 cross-section view of test section with vortex chamber

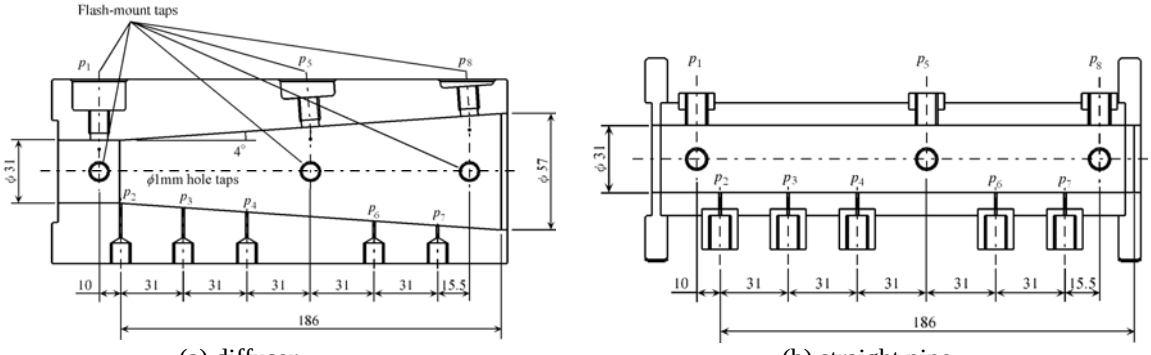

(a) diffuser (b) straight pipe

Fig. 3 geometry and pressure taps displacement of diffuser and straight pipe

Three dynamic pressure transducers p_1, p_5, p_8 are flush mounted along the diffuser and the straight pipe. At the same axial locations but 90° apart in circumferential direction, other three flush mounted pressure transducers are placed to measure the phase difference. Additional static pressure taps p_2, p_3, p_4, p_6 and p_7 were used to measure the pressure distribution along the diffuser, as shown in Fig.3.

The Swirl number Sw is defined to evaluate the swirling intensity in the test section:

$$Sw = \frac{G_\theta}{G_z r_i} = \frac{2\pi\int_0^{r_i}\rho urwrdr}{2\pi\int_0^{r_i}\rho u^2 rdr \cdot r_i} = \frac{2\rho\frac{Q_t}{2}\left(r_t\frac{Q_t}{2A_t}\right)}{\rho\left(\frac{Q}{A_i}\right)^2 A_i \cdot r_i} = \frac{r_t}{2r_i}\frac{A_i}{A_t}\left(\frac{Q_t}{Q}\right)^2$$

where G_θ is the axial flux of angular momentum; G_z is the axial flux of axial momentum; r_i is the inlet radius to the test section; u and w are the axial velocity and tangential velocity. The last expression obtained by assuming the conservation of mass flow and angular momentum gives the nominal value used in the present study: r_t is the distance of tangential inlet from the center of chamber. A_i and A_t are the sectional areas of the test section inlet and the tangential inlet; Q_t and Q are the tangential flow rate and total flow rate respectively.

3. Computational Scheme

The numerical simulation was carried out with the commercial CFD software ANSYS CFX 11.0 package, both for the cases with diffuser and straight pipe. For the spatial discretization, “High-Resolution Scheme” was applied to achieve second order accuracy. For temporal discretization, the second backward Euler scheme was applied. An improved URANS formulation Scalable Adaptive Simulation Shear Stress Transport (SAS SST) model was utilized for turbulence treatment, with the ability to adapt the length scale to resolved turbulent structures. The cavitating simulations were transient, starting from the non-cavitating results with a time-step of 0.001 second, corresponding to about 100 steps per surge period. The simplified Rayleigh-Plesset cavitation model was used. Figure 4 illustrates the computational domain with the diffuser, composed of approximately 1,960,000 structured hexahedral elements. The total flow rate was kept at 150 L/min. At swirl number Sw=1.81, uniform velocity of $u_T = u_R$= 3.54 m/s was assumed at the tangential and radial inlets. Pressure was kept constant at the outlet. The wall boundary condition was imposed to be no slip and smooth wall. The locations of monitoring points are the same as the experiment.

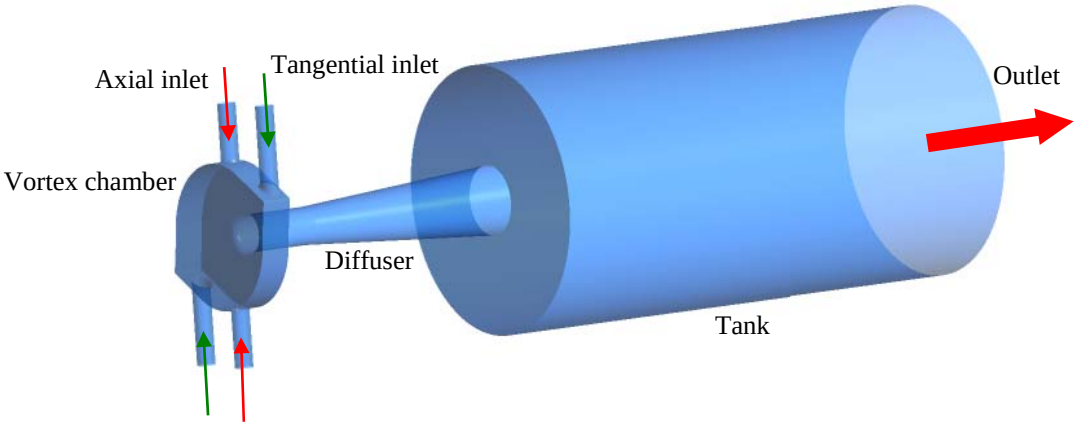

Fig. 4 Computational domain of swirling diffuser flow simulation

4. Results

4.1 Types of fluctuation

Figure 5 shows the Strouhal number St of the pressure fluctuations against the cavitation number σ. The number in the brackets show the phase difference of the fluctuation, measured by the transducers located 90° apart in the circumferential direction. The phase difference of 90° means that one lobe of pressure pattern is rotating in the direction of swirl flow. With swirling flow, a frequency component with St>1 was measured both in the diffuser and straight pipe. Since the circumferential phase difference is 90°, this frequency is considered to be caused by the vortex precession and is called as Type I fluctuation. With diffuser, Type I fluctuation has higher frequency St = 4~6 at p_1 and lower frequency St=1~2 at p_2 and p_3. With straight pipe, it is measured only at p_3, since the cavity quickly extends to the exit of the pipe and the vortex precession occurs only at the pipe exit. Type I fluctuation was simulated by the numerical computation, as shown in Fig.5.

Another fluctuation frequency of St<1 is measured with diffuser, as shown in Fig. 5 (a). It generally occurs at lower cavitation number range, with the circumferential phase difference of 0. This is called Type II fluctuation. Type II fluctuation in the diffuser was also simulated by CFD. By checking the cavity volume V_C, it was found that the fluctuation frequency of V_C agrees with the Type II fluctuation, as shown in Fig.5 (a). In the experiment, it was confirmed that the frequency corresponds to the cavity length fluctuation frequency recorded by high-speed video. Thus, Type II fluctuation is considered to be caused by the cavitation surge. Since it was not found in the straight pipe both in the experiment and simulation, Type II fluctuation is considered to be caused by the diffuser effect, as expected in the one-dimensional analysis [8].In real draft tube model, it has been shown that an intensive surge occurs when the frequency of vortex precession coincides with the natural frequency of the hydraulic system [1]-[3]. Unfortunately, this situation could not be realized in the present smaller size facility.

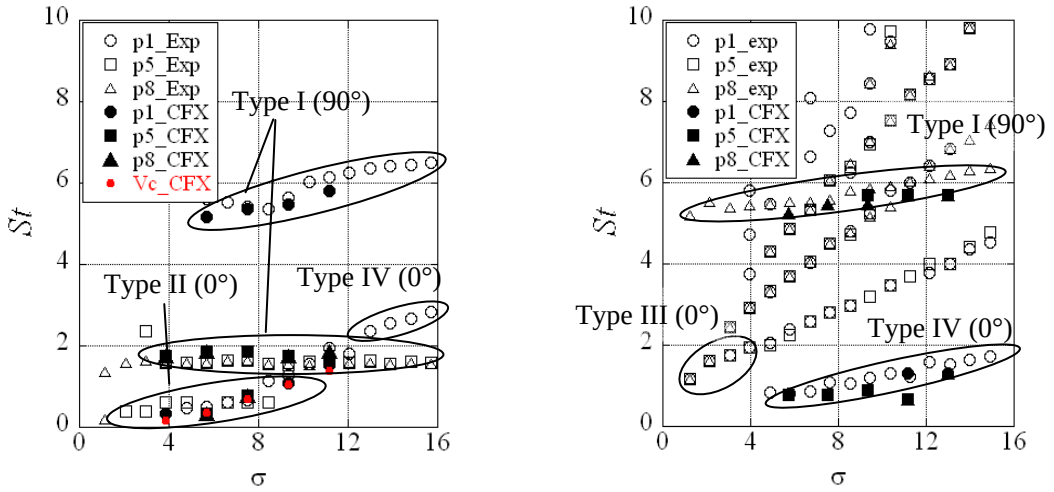

(a) diffuser (b) straight pipe

Fig. 5 Strouhal number *St* against cavitation number σ at *Sw*=1.81

In the straight pipe, another fluctuation frequency was observed at lower cavitation number range of σ<4 with swirling flow, as shown in Fig. 5 (b). Since the high-speed video does not show the cavity length fluctuation with straight pipe, this frequency is different from Type II fluctuation. It is called as Type III fluctuation. The high-speed video shows the measured fluctuation frequency 28 Hz (*St*=1.572) at p_8 agrees with a periodic disturbance which propagates along the cavity surface from downstream to upstream, as shown in Fig.6.

Besides, both in the diffuser and straight pipe, some frequency components which increase with the cavitation number were observed. Due to their weak fluctuation intensity, it is difficult to clarify the mechanism of these oscillations. They are called as Type IV fluctuation in the present study. In the simulation with the straight pipe, a pressure fluctuation was observed, whose frequency agrees well with the lowest series of Type IV fluctuation in the experiment result, as shown in Fig.5 (b). This fluctuation has smaller intensity comparing with Type II fluctuation. It has the largest intensity in the vortex chamber and it decreases when we move downstream in the pipe. Thus, Type IV fluctuation is considered to be caused by the flow in the vortex chamber.

Figure 7 shows the effect of swirl number *Sw* on the Strouhal number *St* under constant cavitation number. With the diffuser and the straight pipe, Type I fluctuation increases with the swirl intensity, while the frequency of Type II fluctuation in the diffuser is almost constant.

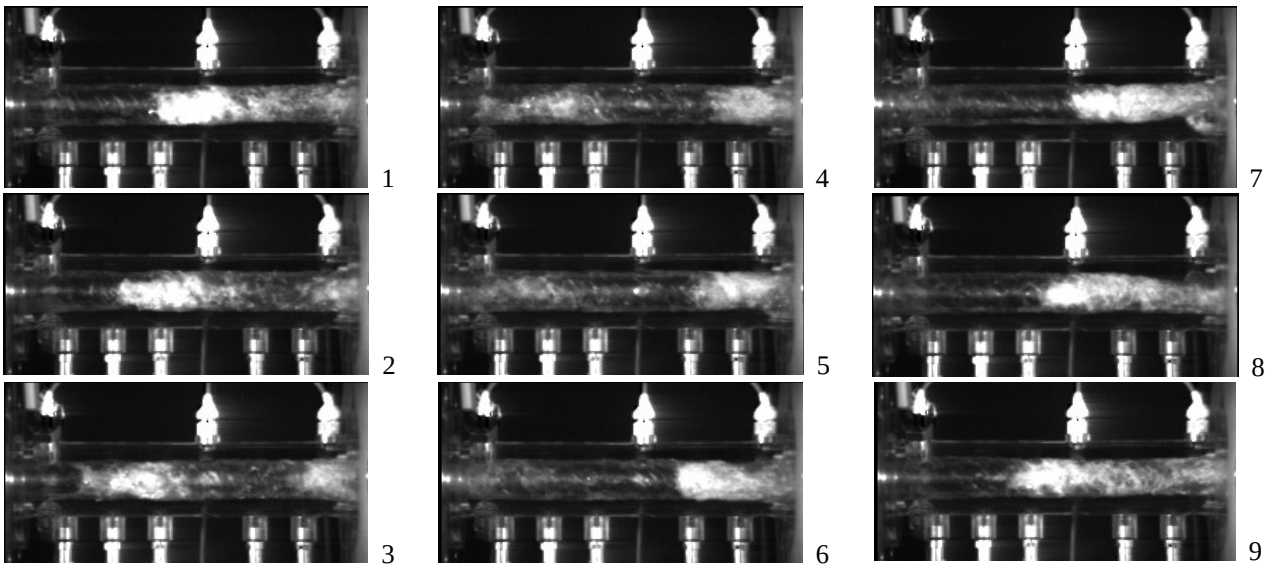

Fig. 6 Disturbance along the cavity from downstream to upstream with straight pipe

(*Sw*=3.21, σ=2.37, Time interval = 0.004444 sec)

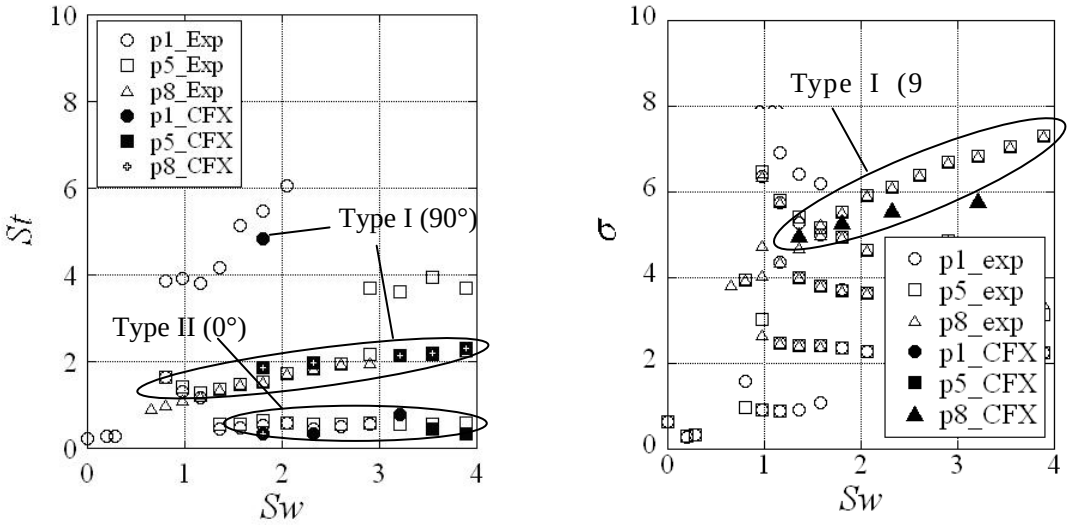

(a) σ=5.65, diffuser (b) σ=5.87, straight pipe

Fig. 7 Effect of swirl number *Sw*

4.2 Cavitation pattern

Figure 8 shows the simulation result with the iso-surface of void fraction f=0.01, comparing with the snapshots in the experiments. The simulation shows that the cavitation is attached at the bottom of the vortex chamber and extends to the diffuser. With straight pipe, it extends to the outlet of the pipe.

The pictures from high-speed video in the experiment at Sw=1.81 and σ=7.52 are shown in Fig.9. The time interval between pictures in Fig. 9 (a) is 0.00222 s. The vortex precession frequency is 90 Hz evaluated from the pictures, corresponding to the Type I fluctuation of 96.43 Hz measured at p_1. The time interval between pictures in Fig. 9 (b) is 0.0222 s. The axial cavity length fluctuation frequency is 11.25 Hz evaluated from the pictures, corresponding to the Type II fluctuation of 10.68 Hz measured at p_1 and p_5.

Figure 10 shows the cross-sectional pressure field at p_1 and p_8 of the diffuser by simulation. The precession of low pressure region is shown. The precession has higher frequency at p_1 (91Hz, St=5.111) and lower at p_8 (31.25 Hz, St=1.755), which are very close to the values evaluated from pressure fluctuation (93.75 Hz, St=5.265 and 33.20 Hz, St=1.864 respectively). It is interesting to note that we can observe a second lower pressure region at p_8 location. Figure 11 shows the iso-surface of void fraction f=0.01 in the diffuser. The cavity length fluctuation (10 Hz, St=0.562) can be observed from the figure, corresponding to the frequency of Type II fluctuation identified in the pressure fluctuation (10.74 Hz, St=0.603). Type III fluctuation was not simulated by the numerical computation.

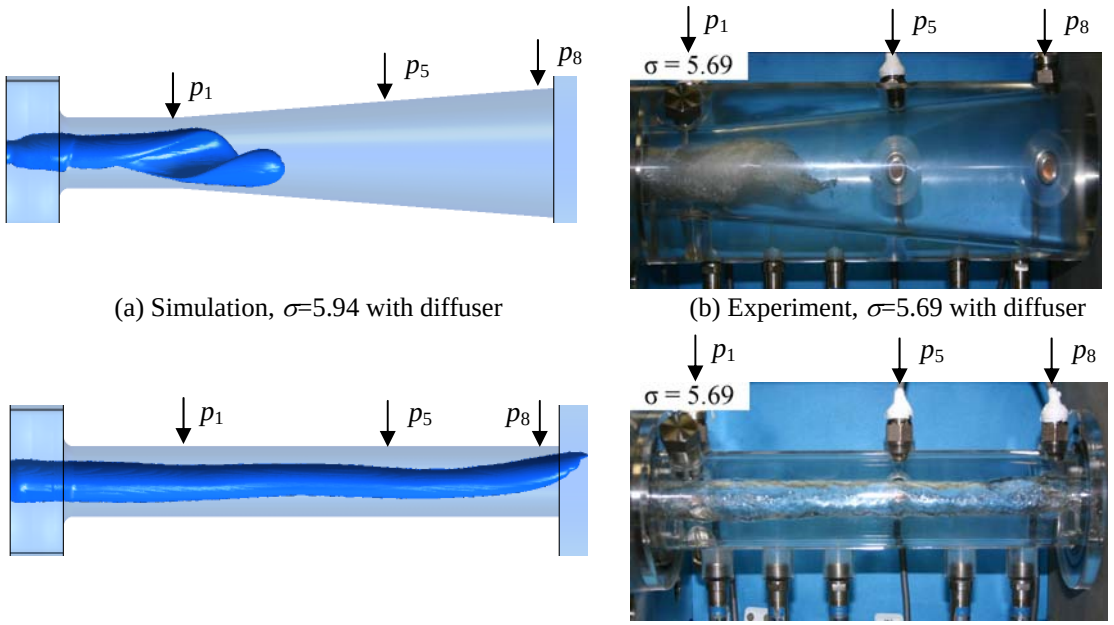

(a) Simulation, σ=5.94 with diffuser (b) Experiment, σ=5.69 with diffuser

(c) Simulation, σ=5.71 with straight pipe (d) Experiment, σ=5.69 with straight pipe

Fig. 8 Typical cavity pattern at Sw=1.81

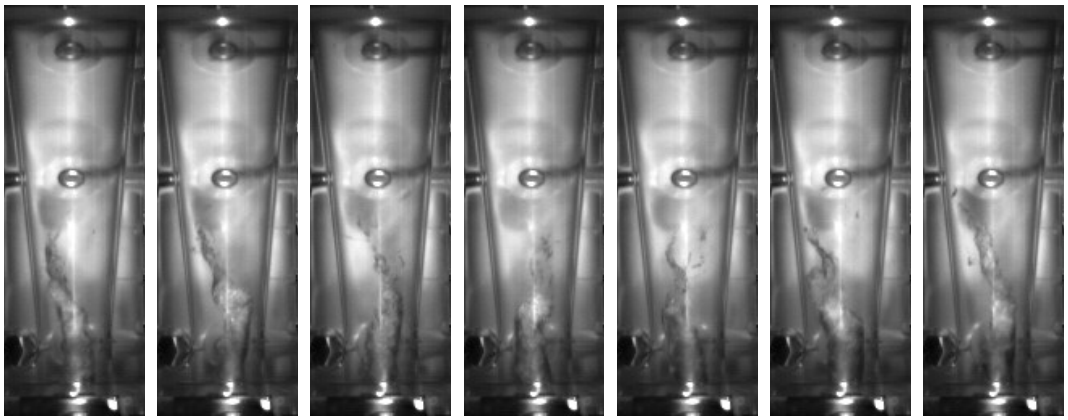

(a) Time interval = 0.00222 s; precession frequency 90 Hz (*St*=5.054)

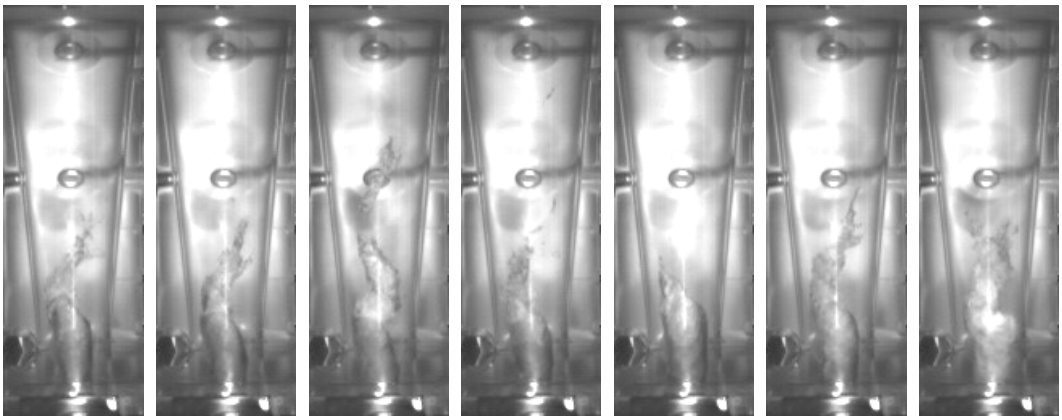

(b) Time interval = 0.0222 s; surge frequency 11.25 Hz (*St*=0.632)

Fig. 9 Experimental snapshots in the diffuser (*Sw*=1.81 and σ=7.52) (2/2)

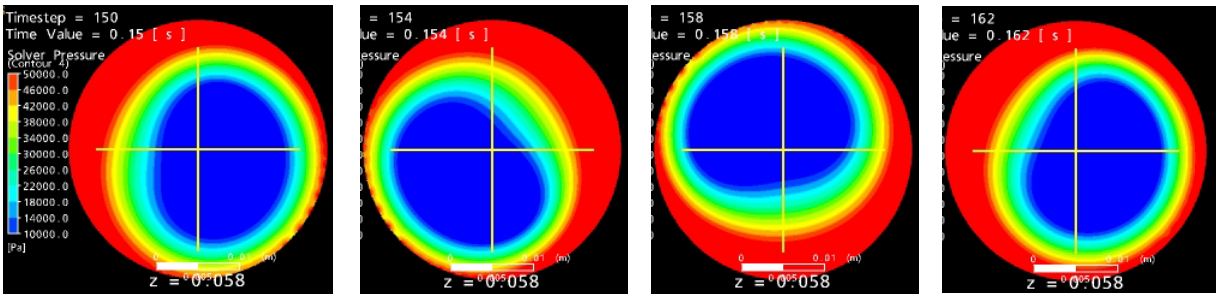

p_1: time interval = 0.004 s; precession frequency 91 Hz (*St*=5.111)

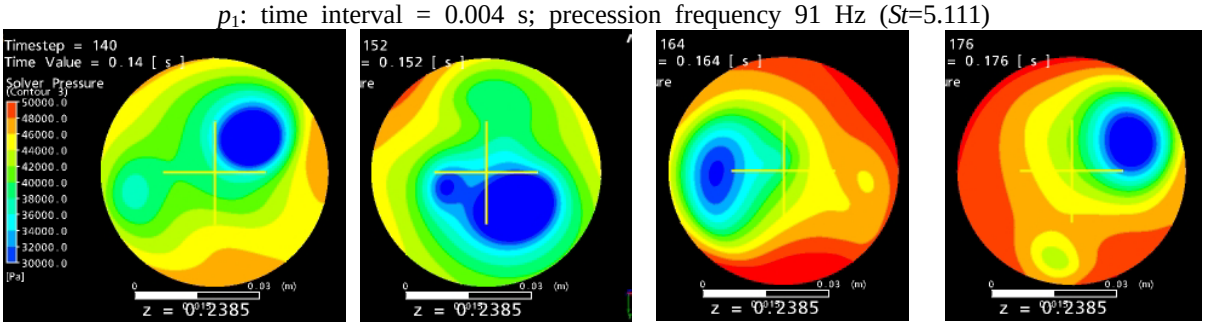

p_8: time interval = 0.012 s; precession frequency 31.25 Hz (*St*=1.755)

Fig. 10 Instantaneous pressure field at cross sections of diffuser (*Sw*=1.81 and σ=7.52)

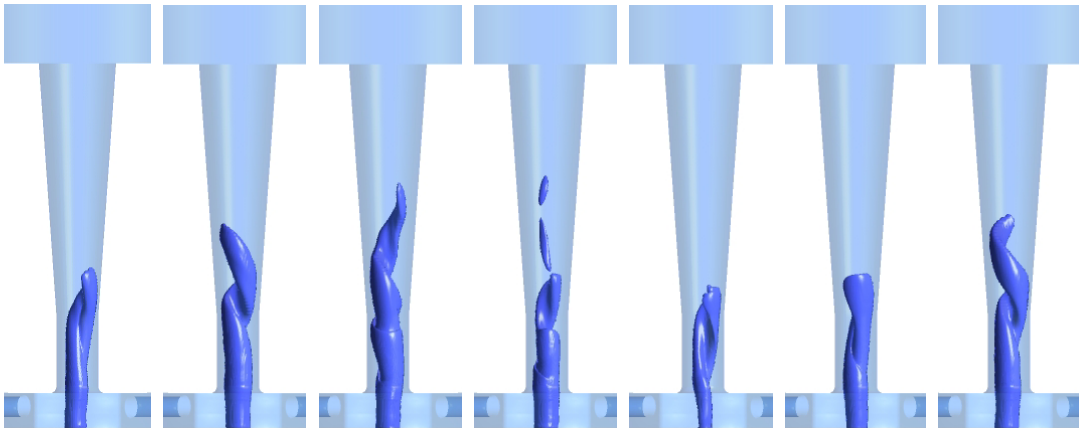

Fig. 11 Instantaneous cavity pattern in the diffuser (Sw=1.81 and σ=7.52)
Time interval = 0.025 s; surge frequency 10 Hz (St=0.562)

4.3 Pressure and velocity distribution

The wall pressure distributions are shown in Fig.12 (a) and (b), from experiments and simulations. The wall pressure decreases towards downstream at higher cavitation numbers both in the diffuser and straight pipe. The pressure recovery caused by the diffuser effect is not clear. Figure 12 (c) and (d) show the pressure distribution along the centerline. With the diffuser, significant pressure recovery occurs over the entire region. The pressure is kept nearly constant with the straight pipe and increase rapidly at the outlet. Figure 12 (e) and (f) show the area averaged pressure distribution. We still observe the pressure recovery for the diffuser. The amount of non-dimensional pressure recovery is larger than 1, suggesting that also the decrease of the tangential velocity is contributing to the pressure recovery. In the one-dimensional model, the pressure recovery due to the decrease of the tangential velocity is not included. The present result shows that also the swirl has a destabilizing effect through the pressure recovery.

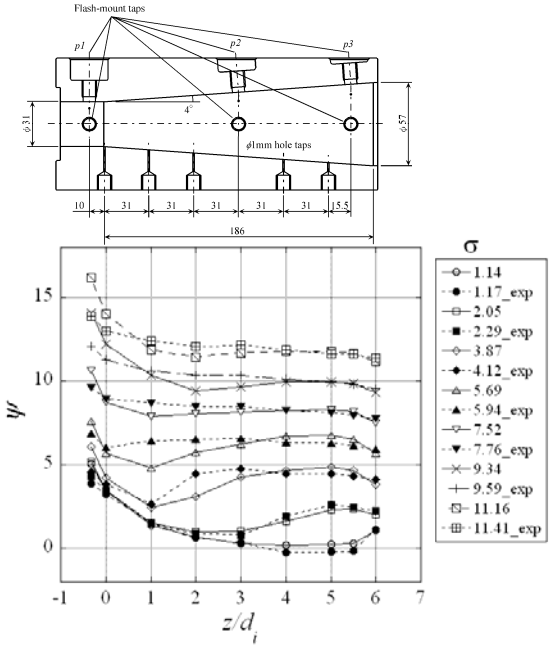

(a) diffuser, wall pressure

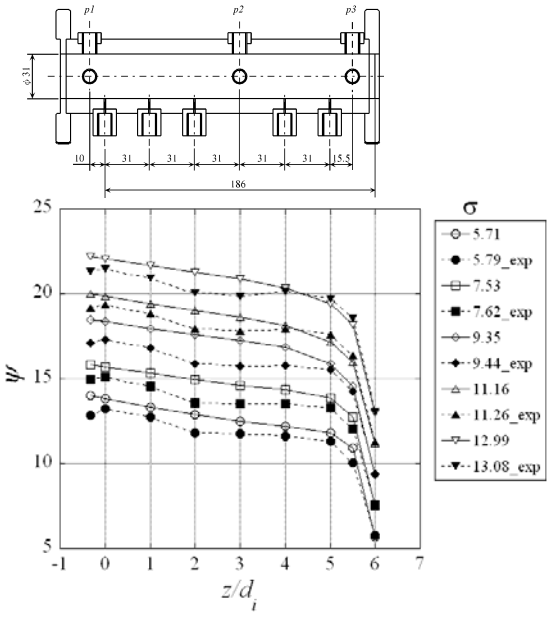

(b) straight pipe, wall pressure

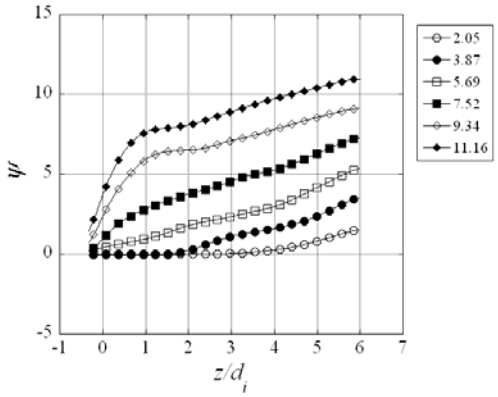

(c) diffuser, along the centerline

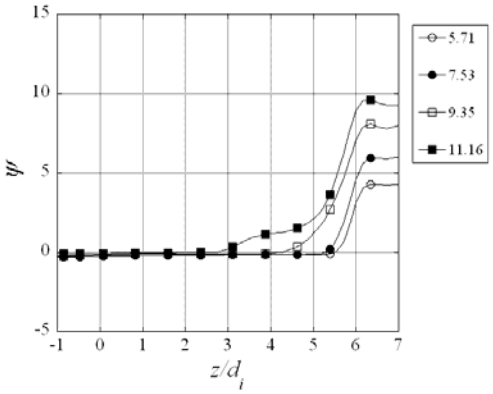

(d) straight pipe, along the centerline

Fig. 12 Axial distribution of Static pressure (1/2)

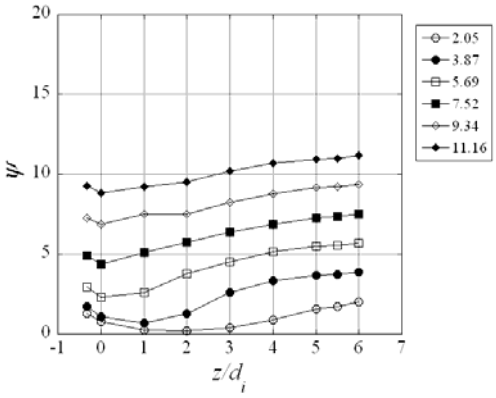

(e) diffuser, cross-sectional average

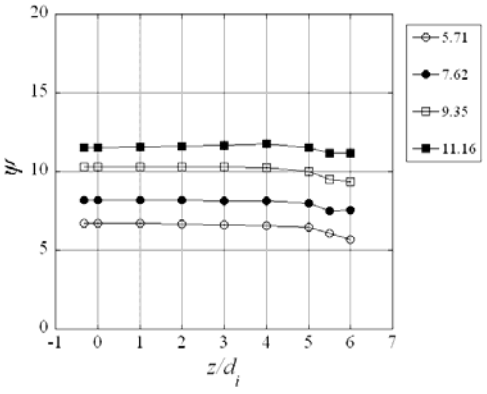

(f) straight pipe, cross-sectional average

Fig. 12 Axial distribution of Static pressure (2/2)

Figures 13 to 16 show the radial distribution of static pressure, tangential and axial velocity, and void fraction at various sections of the diffuser. The tangential velocity distribution is near forced-vortex type. The dashed curves of $r\ u_T$=Const are shown in Fig.14. The results show that the angular momentum or the circulation is kept nearly constant, and it decreases gradually as we proceed downstream. The dash dot lines in Fig.14 show the velocity of precession motion evaluated from the frequency at p_1 (red), p_5 and p_8 (cyan). The precession velocity is higher at p_1, and lower at p_5 and p_8, but close to the flow velocity.

At σ=7.52, the pressure at the center increases rapidly as we proceed downstream. This shows that a substantial pressure recovery occurs although it cannot be observed on the pipe wall. At σ=2.05, the central pressure decreases to ψ=0, corresponding to the increase of void fraction shown in Fig.16. The axial velocity starts to decrease at the radial location where the void fraction starts to decrease. The tangential velocity does not contribute to the radial increase of the pressure in the region where the void fraction is high.

Figure 17 shows the pressure and velocity distribution in the straight pipe. Both the static pressure and tangential velocity near the wall decrease when we proceed downstream.

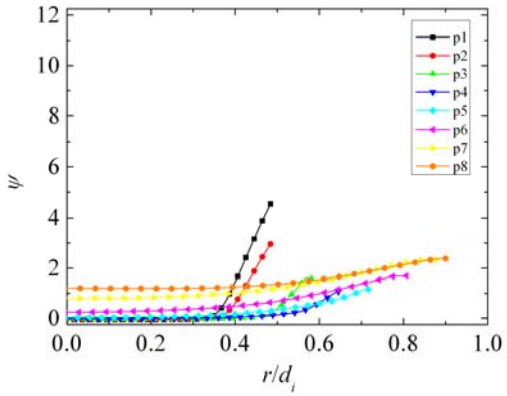

(a) σ = 2.05

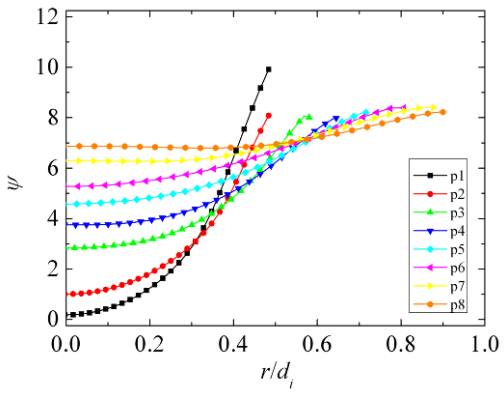

(b) σ = 7.52

Fig. 13 Radial distribution of static pressure (diffuser: *Sw*=1.81)

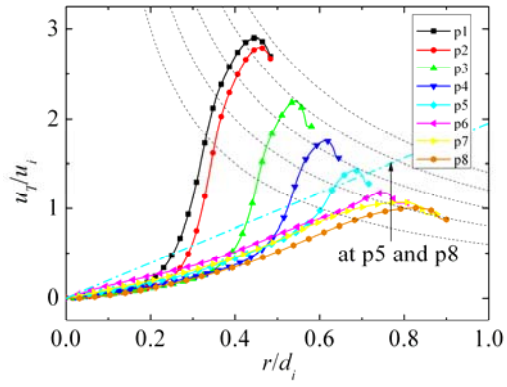

(a) σ = 2.05

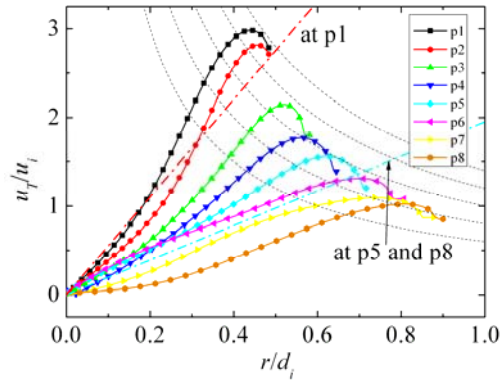

(b) σ = 7.52

Fig. 14 Radial distribution of peripheral velocity (diffuser: *Sw*=1.81)

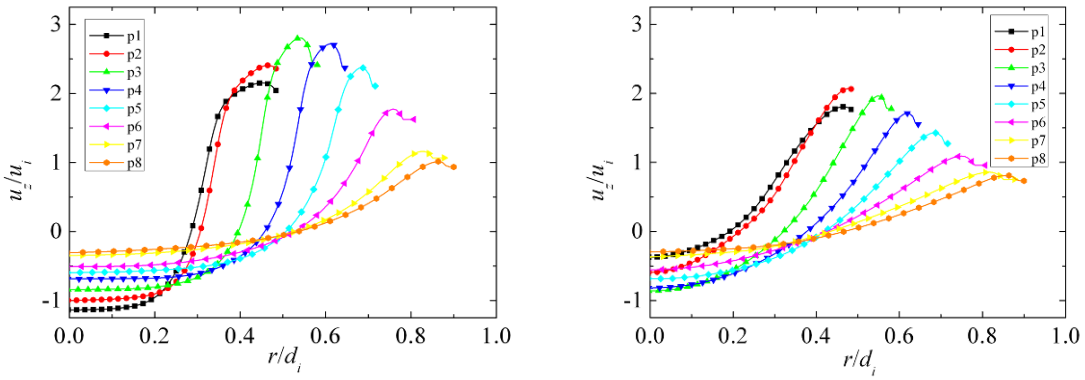

(a) σ = 2.05 (b) σ = 7.52

Fig. 15 Radial distribution of axial velocity (diffuser: *Sw*=1.81)

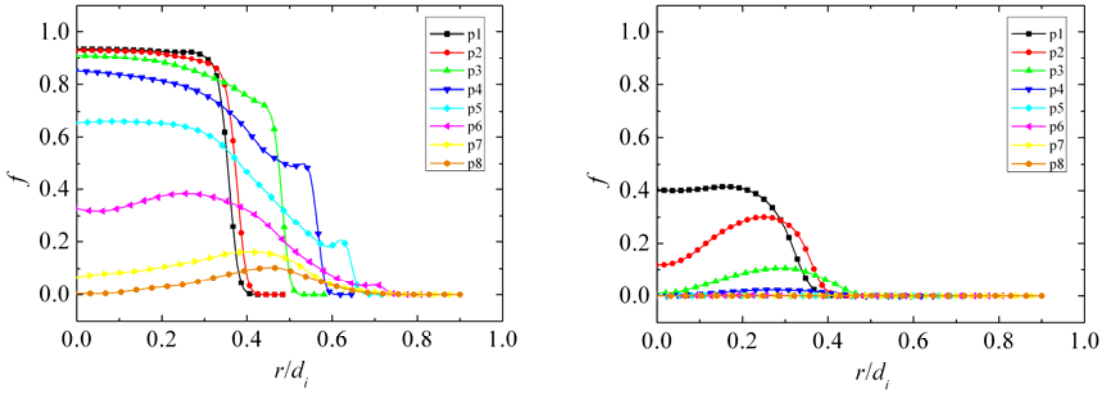

(a) σ = 2.05 (b) σ = 7.52

Fig. 16 Void fraction distribution of axial velocity (diffuser: *Sw*=1.81)

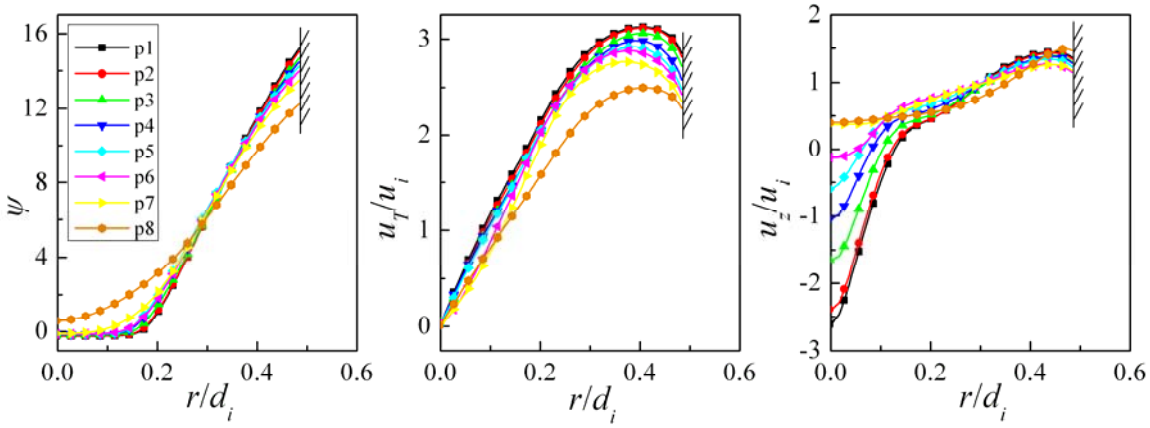

(a) static pressure (b) peripheral velocity (c) axial velocity

Fig. 17 Radial distribution of pressure and velocity in straight pipe (*Sw*=1.81, σ=7.53)

In the experiment with the diffuser, it was found that at lower cavitation number range, the wall pressure at z/d_i<4 was almost constant when decreasing the cavitation number, as shown in Fig.18. The simulation also shows the similar distribution, at σ=2.05 and 1.14 in Fig. 12 (a). Figure 19 shows the radial pressure distribution at z/d_i<4 (p_1~p_4) from simulation results. When we decrease the cavitation number, the pressure near the pipe center decreases to the vapor pressure (ψ=0). Near the wall, the pressure gradient in radial direction is almost the same under various cavitation numbers. At p_1 and p_2, the decrease of the wall pressure is smaller at smaller cavitation number because the increase of the cavitating region with ψ=0 is smaller. Figure 20 shows the iso-curves of time averaged void fraction f_C=0.1. Both the length and diameter of the cavity increases when decreasing the cavitation number. In higher cavitation number range of σ=11.16 to 7.52, the increase of cavity diameter is larger than at the range of σ=5.69 to 2.05, while the increase of cavity length is smaller. Thus, the diameter of cavity region at p_1 is kept constant at σ<3.87, leading to the identical wall pressure in this cavitation number range.

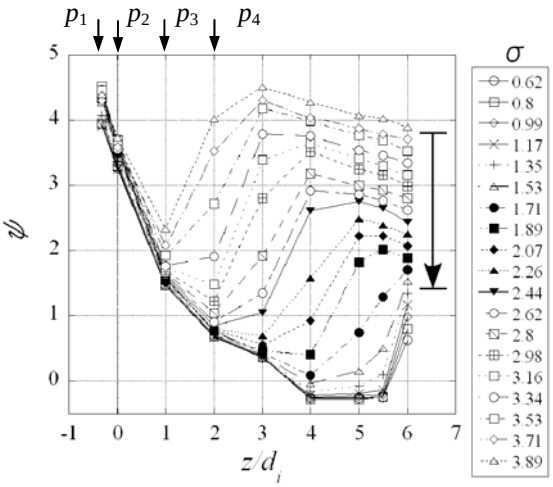

Fig. 18 wall pressure distribution at lower cavitation numbers (diffuser: *Sw*=1.81)

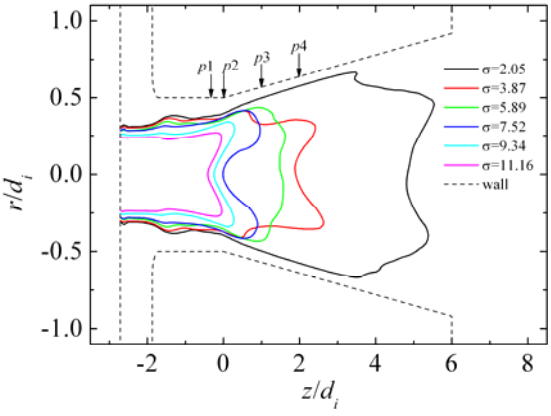

Fig. 20 Iso-curve of time averaged void fraction of f_C=0.1 (diffuser: *Sw*=1.81)

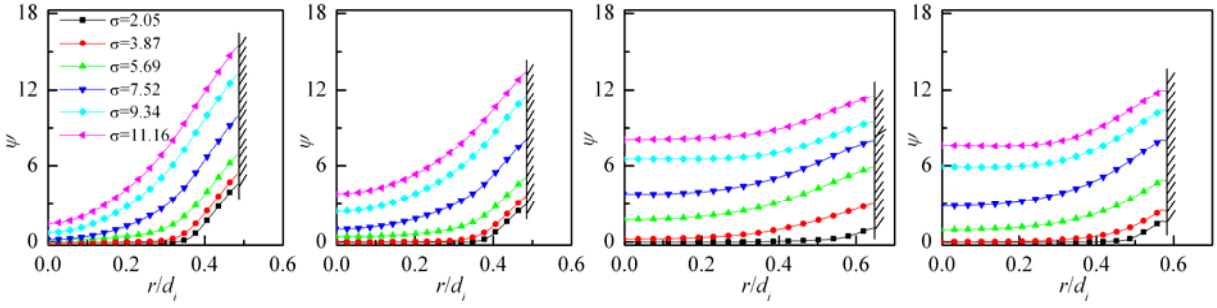

(a) p_1: z/d_i =-0.32 (b) p_2: z/d_i =0 (c) p_3: z/d_i =1 (d) p_4: z/d_i =2

Fig. 19 Static pressure distributions in radial direction (diffuser: *Sw*=1.81)

5. Conclusion

Several types of fluctuation were observed in the experiment with cavitating swirling flow in the diffuser and straight pipe: Type I fluctuation is caused by the vortex precession, observed both in the diffuser and straight pipe. Type II fluctuation is caused by the pressure recovery effect due to the diffuser geometry, which was observed only in the diffuser. Besides, Type III fluctuation caused by the disturbance propagating along the cavity surface, and Type IV fluctuation caused by the vortex chamber were also observed.

Type I and II fluctuations were simulated by the numerical computation. The pressure recovery effect of the diffuser was shown by the axial pressure in the centerline and averaged pressure distribution, although it was not observed by checking the wall pressure distribution. It was shown that the swirling flow has contribution to the pressure recovery.

The radial pressure and velocity distributions showed the swirl was near forced-vortex type. Back flow occurs at the vortex center. The effect of the cavitation on pressure and velocity distributions was examined.

Acknowledgment

The authors would like to thank Mr. Yasuaki Kuwabara and Ms.Sayaka Tanaka, who are former graduate students of Osaka University, for their contribution in the experiment work of this study.

Nomenclature

A_i	Area of diffuser inlet [m^2]	Re	Reynolds Number, = $u_i d_i/\nu$
d_i	Diffuser inlet diameter, 0.031 [m]	r_i	Diffuser inlet radius, 0.0155 [m]
f	Pressure fluctuation frequency [Hz]	r_t	Distance from the center of vortex chamber to the axis of the tangential inlet, 0.0525 [m]
G_θ	Axial flux of angular momentum		
G_z	Axial flux of linear momentum	St	Strouhal number, = fl/u_i
g	Gravitational acceleration constant, 9.81 [kg m/s^2]	Sw	Swirl number, = $G_\theta/(G_z r_i)$
h	Height from diffuser axis to water level [m]	u	Axial velocity [m/s]
l	Diffuser length, 0.186 [m]	u_i	Average inlet velocity [m/s], = Q/A_i
p	Static pressure [Pa]	w	Tangential velocity [m/s]
p_v	Vapor pressure [Pa]	θ	Opening angle of diffuser, 14 [deg]

p_T	Tank pressure [Pa]	ν	Kinematic coefficient of viscosity [m^2/s]
Q	Flow rate [m^3/s]	σ	Cavitation number, = $(p_T-p_v)/(0.5\ \rho u_i^2)$
Q_t	Tangential Flow rate [m^3/s]	ψ	Pressure coefficient, = $(p-p_v)/(0.5\ \rho u_i^2)$

Reference

[1] Nishi, M., "Surging Characteristics of Conical and Elbow Type Draft Tubes," Proceeding of the 12th IAHR Symposium on Hydraulic Machinery and System, Stirling, 1984, pp. 272-283.

[2] Nishi, M., Matsunaga, S., Kubota, T., Senoo, Y., "Flow Regimes in an Elbow-Type Draft Tube," Proceeding of the 11th IAHR Symposium on Hydraulic Machinery and System, Amsterdam, 1982, pp. 1-13, paper 38.

[3] Nishi, M., Wang, X., Okamoto, M., Matsunaga, S., "Further Investigation on the Pressure Fluctuations Caused by Cavitated Vortex Rope in an Elbow Draft Tube," In Cavitation and Gas Fluid Flow Machinery and Devices (1994), ASME, pp. 63-70.

[4] Prenat, J-E., Jacob, T., "Investigating the Behavior at High Load of a Francis Turbine Model," 13th IAHR Symposium, Montreal, 1986.

[5] Arzola, F., Azuaje, C., Zambrano, P., Gulbrandsen, G., "Undesired Power Oscillations at High Load in Large Francis Turbines. Experimental Study and Solution," 23rd IAHR Symposium, Yokohama, 2006

[6] Koutnik, J., Pulpitel, L., "Modeling of the Francis Turbine Full-Load Surge," Modeling, Testing and Monitoring for Hydro Power Plants, Lausanne, 1996.

[7] Koutnik, J., Nicolet, C., A.Schoul, G., Avellen, F., "Overload Surge Event in a Pumped- Storage Power Plant," 23rd IAHR Symposium, Yokohama, 2006.

[8] Chen, C., Nicolet, C., Yonezawa, K., Farhat, M., Avellen, F., Tsujimoto, Y., "One-Dimensional Analysis of Full Load Draft Tube Surge," ASME Journal of Fluids Engineering, vol.130, Issue 4, 041106.

[9] Chen, C., Nicolet, C., Yonezawa, K., Farhat, M., Avellen, F., Miyazawa, K., Tsujimoto, Y., "Experimental Study and Numerical Simulation of Cavity Oscillation in a Conical Diffuser," Submitted to International Journal of Fluid Machinery and System, 2010.